Available online at www.sciencedirect.com
SCIENCE DIRECT
Journal of Catalysis 237 (2006) 322–329
JOURNAL OF CATALYSIS
www.elsevier.com/locate/jcat

Sulfur-substituted and zinc-doped $In(OH)_3$: A new class of catalyst for photocatalytic H_2 production from water under visible light illumination

Zhibin Lei [a], Guijun Ma [a], Meiying Liu [a], Wansheng You [a], Hongjian Yan [a], Guopeng Wu [a], Tsuyoshi Takata [b], Michikazu Hara [b], Kazunari Domen [b,c,*], Can Li [a,*]

[a] *State Key Laboratory of Catalysis, Dalian Institute of Chemical Physics, Chinese Academy of Sciences, Dalian, 116023, China*
[b] *Chemical Resource Laboratory, Tokyo Institute of Technology, Nagatsuta 4259, Midoni-ku, Yokohama 226-8503, Japan*
[c] *Solution Oriented Research for Science and Technology, Japan Science and Technology Corporation(SORST, JST), 2-1-13 Higashiueno, Taito-ku, Tokyo 110-0015, Japan*

Received 28 August 2005; revised 10 November 2005; accepted 20 November 2005

Abstract

Sulfur-substituted $In(OH)_3$ [hereafter denoted as $In(OH)_yS_z$] and Zn-doped $In(OH)_yS_z$ [hereafter denoted as $In(OH)_yS_z$:Zn] are synthesized in an aqueous solution of ethylenediamine via the hydrothermal method. The photoactivities of these catalysts for H_2 production are investigated in the presence of Na_2S and Na_2SO_3 sacrificial reagent under visible light illumination ($\lambda > 420$ nm). The absorption edge of $In(OH)_yS_z$ shifted monotonically from 240 nm for $In(OH)_3$ to 570 nm for $In(OH)_yS_z$ when the atomic ratio of S/In in the synthesis solution is increased from 0 to 2.0. But the absorption edge of $In(OH)_yS_z$:Zn shifted from 570 to 470 nm as the atomic ratio of Zn/In in the synthesis solution was increased from 0 to 1.0. The catalyst $In(OH)_yS_z$ is active for H_2 production, with an average rate of H_2 of 0.9–1.8 μmol/h, under visible light illumination. The photoactivity of $In(OH)_yS_z$ is enhanced by doping with Zn^{2+}. The rate of H_2 production is 35.8 and 67 μmol/h on 2wt% Pt-loaded $In(OH)_yS_z$:Zn catalyst when $X = 0.2$ and 0.5, respectively, corresponding to a quantum efficiency of 0.32 and 0.59% at 420 ± 10 nm, respectively.

Keywords: $In(OH)_yS_z$; Zn^{2+} doping; Hydrogen production; Photocatalysis

1. Introduction

Photocatalytic water splitting into H_2 and O_2 using semiconductor photocatalysts has received much attention because it has been considered an ideal method to address energy and environmental problems. Many effective photocatalysts in the ultraviolet (UV) region have been developed for overall water splitting [1–5]. Developing highly active photocatalysts with a visible light response to use solar energy is important, because visible light composes the major part of the solar spectrum.

Over the last few years, considerable effort has been made to increase the absorption of catalysts in the visible region to improve visible light response; approaches have included single-phase oxide photocatalyst $CaBi_2O_4$ for organic contaminant decomposition [6] and $PbBi_2Nb_2O_9$ for both isopropyl alcohol degradation and water decomposition [7]. One effective way to narrow the band gap is to elevate the valence band of photocatalysts into a more negative position by anion substitution. For example, Asahi et al. reported a nitrogen-doped TiO_2 that shifted its optical absorption to the visible region and enhanced the photoactivity for the degradation of methylene blue and gaseous acetaldehyde [8]. Khan et al. reported a $TiO_{2-x}C_x$ catalyst with higher photocurrent density and photoconversion efficiency for water splitting [9]. Very recently, N^{3-} and S^{2-} substituted metal–oxide catalysts, including TaON, Ta_3N_4, $LaTiO_2N$, $Y_2Ta_2O_5N_2$, and $Sm_2Ti_2S_2O_5$, have been reported as the visible light-responsive catalysts for water reduction and/or oxidation in the presence of a sacrificial electron donor (methanol) or acceptor (Ag^+) [10–14]. On the other hand, the absorption edge of photocatalysts can also be shifted into the visible region by forming donor levels in the

* Corresponding authors. Fax: +81 3 5841 8838 (K. Domen), +86 411 84694447 (C. Li).
E-mail addresses: kdomen@res.titech.ac.jp (K. Domen), canli@dicp.ac.cn (C. Li).

0021-9517/$ – see front matter
doi:10.1016/j.jcat.2005.11.022

forbidden band. ZnS doped with Cu and Ni and ZnS co-doped with Pb and halogens show quite high activity for H_2 evolution in the visible region [15–17]. In particular, the $InTaO_4$ doped with Ni was found to be an active photocatalyst for overall water splitting in the visible light region [18].

The polynary metal sulfides and oxysulfides are reportedly stable photocatalysts for water reduction and/or oxidation [19–21]. The recently reported solid solution catalysts ZnS–$CuInS_2$–$AgInS_2$ and $(AgIn)_xZn_{2(1-x)}S_2$ showed quite high photoactivity of H_2 evolution in aqueous solution of Na_2S and K_2SO_3 [22,23], with apparent quantum yield as high as 20% in the visible region under optimal preparation conditions. The high photoactivity of the $(AgIn)_xZn_{2(1-x)}S_2$ catalyst is related to its high potential level of the conduction band consisting primarily of Zn 4s4p. The conduction band with high potential level provides a large thermodynamic driving force for water reduction.

It has been reported that calcium hydroxyapatite modified with Ti(IV) can be used as a photocatalyst for albumin decomposition under UV illumination [24]. But the photoactivity of this kind of catalyst has not been reported for water reduction. $In(OH)_3$ is a semiconductor with wide band gap (B.G. 5.17 eV) and absorption in the deep UV region. The wide band gap is related to its deep potential level of O 2p orbital. Due to the higher energy level of S 3p compared with O 2p, substitution of S^{2-} for O^{2-} to elevate the valence band is one potential way to narrow the band gap of metal oxides. Recently, sulfur-substituted $In(OH)_3$ prepared by chemical bath deposition has shown promising applications in solar cells [25–29]. In the present work, we report the visible light-responsive $In(OH)_yS_z$ photocatalyst by controlling the substitution amount of S^{2-} for OH^- via the hydrothermal method at 180 °C. The band structure of $In(OH)_yS_z$ was tuned by Zn^{2+} cation doping. The photoactivity of H_2 production on both $In(OH)_yS_z$ and $In(OH)_yS_z$:Zn was investigated under visible light illumination in the presence of Na_2S and Na_2SO_3 aqueous solution. It was found that the absorption edge of $In(OH)_3$ is shifted monotonically from 240 nm to a longer wavelength when more OH^- was replaced by S^{2-}. The $In(OH)_yS_z$ synthesized by substituting OH^- with S^{2-} is active for H_2 production, and its photoactivity is further enhanced by doping with Zn^{2+}. The factors influencing photoactivity are discussed, and the possible band structure of $In(OH)_yS_z$:Zn is described.

2. Experimental

2.1. Catalyst preparation

The photocatalysts were prepared by hydrothermal synthesis methods. All of the reagents were analytical grade and used without further purification. The $In(OH)_3$ was prepared with $In_2(SO_4)_3$ as the only precursor in a 30-mL Teflon-lined stainless steel autoclave. For the preparation of $In(OH)_yS_z$ and $In(OH)_yS_z$:Zn, desired amounts of thiourea and $Zn(NO_3)_2 \cdot 6H_2O$ were added. In what follows, the value of X is used to describe the nominal atomic ratio of Zn/In for $In(OH)_yS_z$:Zn in the synthesis solution. All of the autoclaves were filled with an appropriate amount of ethylenediamine; then double-distilled water was added to form an aqueous solution of ethylenediamine. The autoclave was maintained at 180 °C for 20 h. The products were collected by filtration and washed several times with water and ethanol. After drying at 80 °C, the yellow precipitates were obtained.

2.2. Catalyst characterization

UV–visible light (UV–vis) diffuse reflectance spectra were recorded on a JASCO V-550 UV–vis spectrophotometer equipped with an integrating sphere. The structure and the phase of the sample were determined by X-ray diffraction (XRD) with a Rigaku D/max-2500 diffractometer using Cu-K_α radiation, with an operation voltage of 40 kV and an operating current of 100 mA. The scan rate of 8°/min was applied to record the patterns in the range of 10–82° at a step size of 0.02°. The elemental analysis was conducted on Plasam-Spec-II inductively coupled plasma atomic emission spectrometer. Nitrogen adsorption–desorption measurements were performed at 77 K on a Micromeritics ASAP 2000 system to obtain the Brunauer–Emmett–Teller (BET) surface area. Before measurement, all samples were degassed at 150 °C overnight. Thermogravimetric analysis (TGA) and differential thermal (DTA) analysis were carried out under a nitrogen stream at a heating rate of 10 °C/min, using a Pyris Diamond thermogravimetric/differential thermal analyzer.

2.3. Photocatalysis reaction

The photoactivities of the samples were examined in a closed gas circulation and evacuation system. Typically, 0.3 g powder of catalyst was dispersed in a Pyrex reaction cell containing 200 mL of an aqueous solution of 0.43 M Na_2S and 0.5 M Na_2SO_3. 2wt% Pt co-catalyst was loaded on the photocatalyst by in situ photochemical deposition from H_2PtCl_6 aqueous solution. The light source was a 300-W Xe lamp equipped with an optical cutoff filter ($\lambda > 420$ nm). A shutter window and a water filter were placed between the Xe lamp and the reaction cell to remove infrared (IR) light illumination. The amount of the produced H_2 was analyzed using on-line gas chromatography (with a thermal conductivity detector and an Ar carrier). The apparent quantum efficiency was measured using filters combined with a bandpass and a Si photodiode. The rate of total photons reaching the solution was typically 1.49×10^{21} photons $\cdot\, h^{-1}$ at $\lambda = 420 \pm 10$ nm. The quantum efficiency value (Φ) was calculated using the following equation:

$$\Phi\ (\%) = (AR/I) \times 100,$$

where A, R, and I represent the coefficients based on the photoreactions (for H_2 evolution, $A = 2$), the H_2 evolution rate at 420 ± 10 nm (molecules h^{-1}), and the rate of absorption of incident photons, respectively. Here Φ is the apparent quantum efficiency, because we assume that all of the incident photons are absorbed by the catalyst.

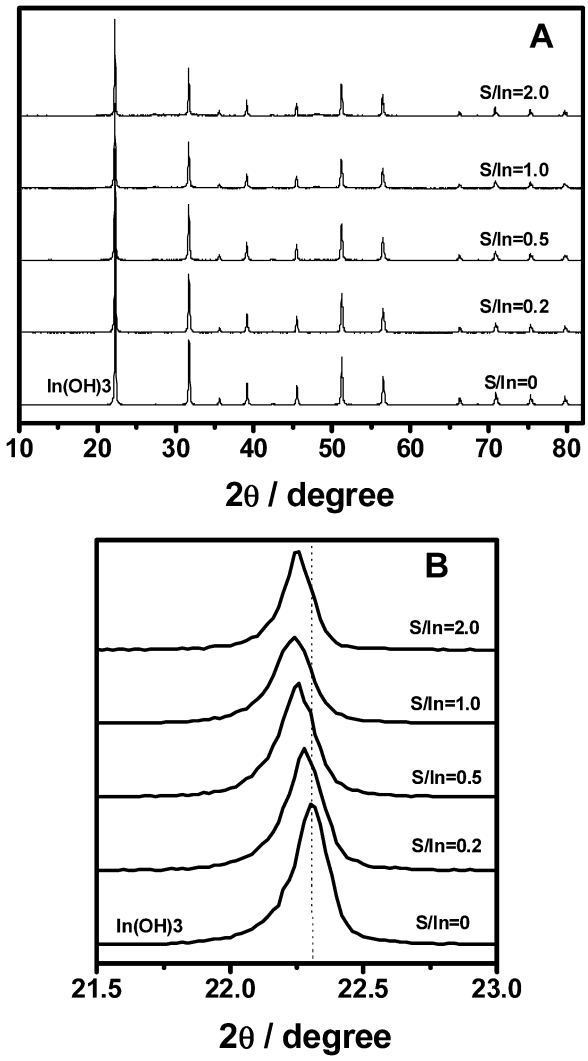

Fig. 1. Powder X-ray diffraction patterns of $In(OH)_3$ and $In(OH)_yS_z$ with S/In atomic ratio varied from 0.2 to 2.0 in the synthesis solution. All the catalysts were synthesized in aqueous solution of ethylenediamine at 180 °C for 20 h.

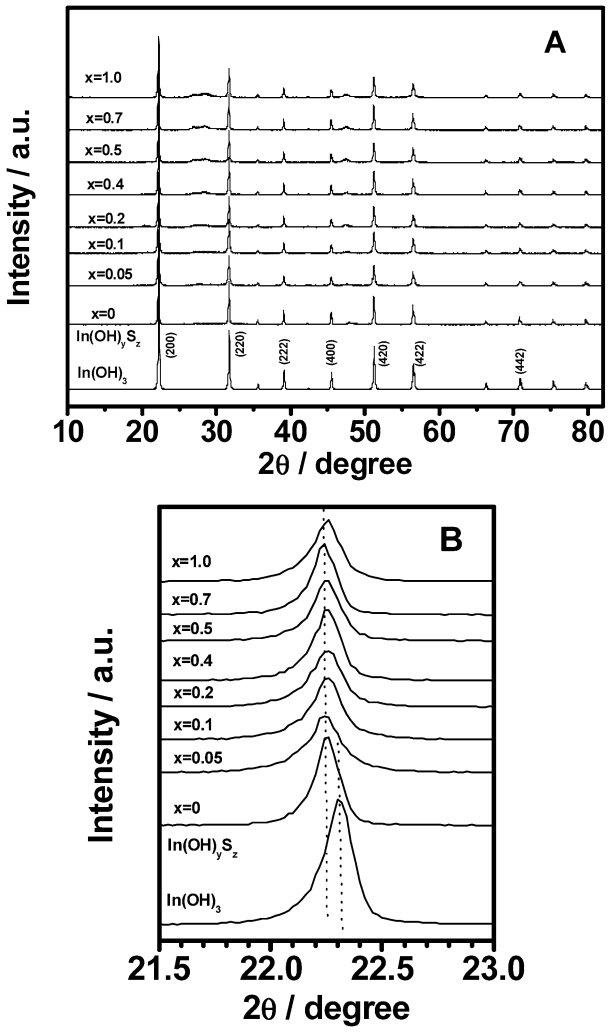

Fig. 2. Powder X-ray diffraction patterns of $In(OH)_3$, $In(OH)_yS_z$ and $In(OH)_yS_z$:Zn (X denoted the atomic ratio of Zn/In in the synthesis solution) synthesized in aqueous solution of ethylenediamine at 180 °C for 20 h.

3. Results and discussion

3.1. XRD pattern of $In(OH)_3$, $In(OH)_yS_z$, and $In(OH)_yS_z$:Zn

Fig. 1A shows the XRD pattern of $In(OH)_3$ and $In(OH)_yS_z$ synthesized in an aqueous solution of ethylenediamine with the atomic ratio of S/In of 0.2–2 in synthesis solution. In the absence of thiourea (S/In = 0), the diffraction peaks of the obtained sample can be readily indexed to a pure phase of cubic $In(OH)_3$ with calculated lattice constant $a = 7.959$ Å, in agreement with previously reported values (JCPDS 85-1338; $a = 7.979$ Å). The diffraction peaks are intense and sharp, indicating that the obtained $In(OH)_3$ is well crystallized under the present hydrothermal condition. When S^{2-} is partially substituted for OH^-, the obtained $In(OH)_yS_z$ exhibits almost the same XRD patterns as that of cubic $In(OH)_3$ except the diffraction peaks are slightly shifted to low angles, as shown in Fig. 1B. In addition, the diffraction peaks shifted to much lower angles with the increasing S/In ratio in the synthesis solution. When the ratio of S/In exceeded 2, the diffraction peaks had no distinct shift, and a diffraction peak characteristic of β-In_2S_3 appeared. This observation suggests that S^{2-} was homogeneously incorporated into the lattice of $In(OH)_3$ and located at OH^- sites. This is a reasonable suggestion, because the ionic radius of S^{2-} (1.84 Å) is larger than the thermochemical radius of OH^- (1.40 Å).

$In(OH)_yS_z$ doped with Zn^{2+} was synthesized via the same hydrothermal method as for $In(OH)_yS_z$, with the atomic ratio of S/In kept at 2 in the synthesis solution. XRD patterns of $In(OH)_yS_z$ doped with different amounts of Zn^{2+} are shown in Fig. 2A. The diffraction peaks also display a similar XRD pattern as seen for $In(OH)_yS_z$. But with the value of X increased from 0 to 1, the peaks of $In(OH)_yS_z$:Zn shift slightly to larger angles, as shown in Fig. 2B, suggesting that Zn^{2+} is homogeneously located at the In^{3+} position in the lattice of $In(OH)_yS_z$. This is due to the slightly different ionic radius of Zn^{2+} (0.74 Å) and In^{3+} (0.81 Å).

As a semiconductor, $In(OH)_3$ is generally prepared by hydrolyzing In^{3+} or oxidizing indium metal in NaOH aqueous solution [30–32]. In this work, the aqueous solution of ethylene-

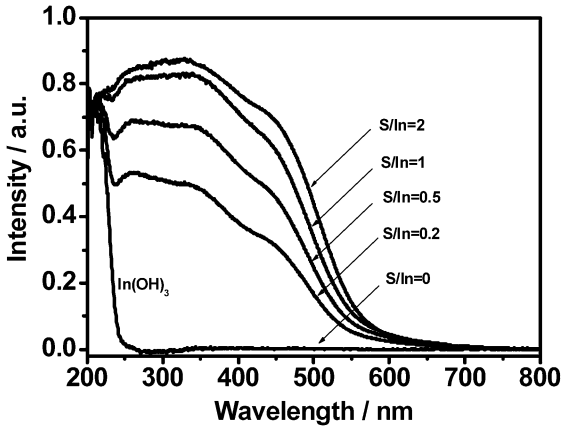

Fig. 3. UV–vis diffuse reflectance spectra of $In(OH)_3$ and $In(OH)_yS_z$ with S/In atomic ratio varied from 0.2 to 2.0 in the synthesis solution.

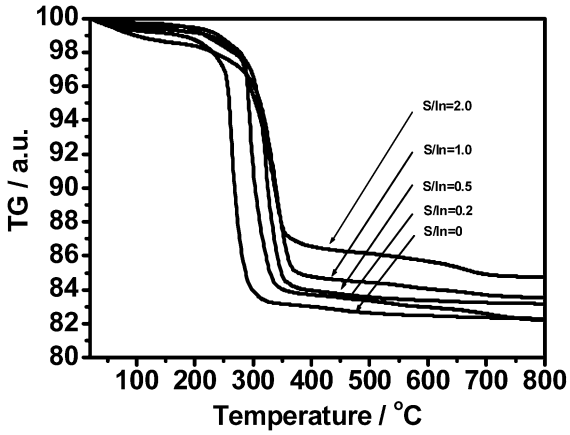

Fig. 4. Thermogravimetric analysis of $In(OH)_3$ and $In(OH)_yS_z$ with S/In atomic ratio varied from 0.2 to 2.0 in the synthesis solution.

diamine is used as a reaction medium to provide the necessary alkaline for the hydrolysis of In^{3+}. In the presence of low substitution amounts of S^{2-}, pure-phase $In(OH)_yS_z$ is obtained. At high Zn/In ratios for the synthesis of $In(OH)_yS_z$:Zn, S^{2-} reacts with Zn^{2+} to produce ZnS. As shown in Fig. 2A, the diffraction peaks of ZnS with characteristics of wurtzite structure occurred with increasing values of X. This observation demonstrates that a minimum amount of ZnS was formed on the surface of $In(OH)_yS_z$.

3.2. UV–vis diffuse reflectance spectra and thermogravimetric analysis

Fig. 3 shows the UV–vis diffuse reflectance spectra of $In(OH)_3$ and $In(OH)_yS_z$ with varying S/In atomic ratios in the synthesis solution. The onset of the absorption edge of $In(OH)_3$ is at 240 nm, corresponding to the band gap of 5.17 eV. This value is consistent with the band gap reported by Avivi et al. [33]. With increasing S/In atomic ratio in the synthesis solution, the absorption of $In(OH)_yS_z$ increased in intensity, and its edge shifted to the visible region. The red shift of the absorption edge with the increase of S/In ratio suggests that more OH^- was substituted with S^{2-}. The band gap estimated from the onset of absorption edge changed from 5.17 eV for $In(OH)_3$ to 2.19 eV when the S/In atomic ratio increased from 0 to 2 in the synthesis solution.

TGA was carried out to analyze the thermal behavior of catalyst; the profiles of $In(OH)_yS_z$ are shown in Fig. 4. A pronounced weight loss step occurred in the temperature range of 200–500 °C. The observed weight loss for the transformation of $In(OH)_3$ into In_2O_3 was 16.1%, in good agreement with the theoretical value of 16.3%. The slight weight loss above 550 °C can be presumptively ascribed to the decomposition of the absorbed ethylenediamine molecules on the surface of $In(OH)_3$. At 200–500 °C, however, the weight loss of $In(OH)_yS_z$ decreased, and the corresponding endothermic peaks shifted to higher temperatures when more OH^- was substituted with S^{2-}. The increased decomposition temperature for $In(OH)_yS_z$ with increasing S/In ratio is possibly related to the large difference in the standard formation enthalpy between In_2S_3 and In_2O_3 ($\Delta_r H^\circ_m = -427$ kJ/mol for In_2S_3 and -925.27 kJ/mol for In_2O_3). The decreased weight loss at high S/In ratio can be attributed to the substitution of S^{2-} for more OH^- in the lattice of $In(OH)_3$, if the decomposition of $In(OH)_yS_z$ proceeds according to the following process:

$$2In(OH)_{3-x}S_{x/2} \rightarrow In_2O_{3-x}S_x + (3-x)H_2O.$$

Based on the weight loss of $In(OH)_yS_z$, it is possible to estimate the amount of S substituted and to determine the molecular formula of $In(OH)_yS_z$. The observed weight loss, band gap, and possible molecular formula for $In(OH)_yS_z$ are summarized in Table 1. With the S/In atomic ratio was changed from 0.2 to 2, the S/In ratio in the $In(OH)_yS_z$ product increased, but to a much less degree than the S/In atomic ratio in the synthesis solution. Despite this, the substitution of OH^- with minimum S^{2-} led to a dramatic shift of the absorption edge into the visible region, as shown in Fig. 3. This is reasonable, because S 3p has more negative energy than the O 2p orbital. The red shift of the absorption edge for $In(OH)_yS_z$ into the visible region with increasing S/In atomic ratio is consistent with the shift of diffraction peaks to lower angles shown in Fig. 1B.

Table 1
The physical parameter and the photoactivity of H_2 production on $In(OH)_yS_z$ under visible light illumination ($\lambda > 420$ nm)

Atomic ratio of S/In in synthesis solution	Weight loss[a] (%)	Possible molecular formula[b]	Bang gap[c] (eV)	The rate of H_2 production[d] (μmol/h)
0	16.1	$In(OH)_3$	5.17	0
0.2	15.9	$In(OH)_{2.92}S_{0.04}$	2.25	0.9
0.5	15.6	$In(OH)_{2.87}S_{0.06}$	2.23	1.8
1.0	14.2	$In(OH)_{2.62}S_{0.19}$	2.20	1.5
2.0	12.6	$In(OH)_{2.32}S_{0.34}$	2.19	1.4

[a] Weight loss in 200–400 °C calculated from TGA analysis.
[b] Molecular formula obtained by supposing the decomposition of $In(OH)_yS_z$ according to the following process: $2In(OH)_{3-x}S_{x/2} \rightarrow In_2O_{3-x}S_x + (3-x)H_2O$.
[c] Band gap estimated from the onset of the absorption edge.
[d] The average rate in 10 h photoreaction.

Fig. 5 shows the UV–vis diffuse reflectance spectra of ZnS and $In(OH)_yS_z$ doped with varying amounts of Zn^{2+}. The absorption edge of $In(OH)_yS_z$:Zn is located between that of ZnS

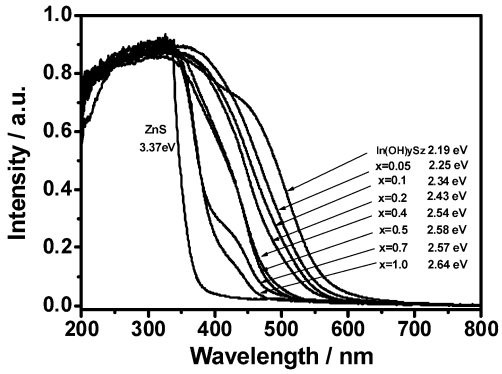

Fig. 5. UV–vis diffuse reflectance spectra of ZnS, $In(OH)_ySz$ and $In(OH)_ySz$:Zn catalysts with different X value (X denotes the atomic ratio of Zn/In in the synthesis solution). The $In(OH)_ySz$ and $In(OH)_ySz$:Zn were obtained with atomic ratio of S/In = 2.0.

and $In(OH)_ySz$ and shifts monotonously from 566 to 470 nm with an increase in X from 0 to 1.0, corresponding to the increase in band gap from 2.19 to 2.64 eV. With X changed from 0 to 1, the band of $In(OH)_ySz$:Zn displays two types of absorption characters. No absorption ascribed to the ZnS is observed at low Zn doping ($X \leqslant 0.5$), confirming that the Zn^{2+} is homogeneously doped in the lattice of $In(OH)_ySz$. Moreover, $In(OH)_ySz$:Zn with low Zn doping ($X \leqslant 0.5$) exhibits steep edges and strong absorption in the visible light region, suggesting that the absorption is due to the transitions between the valence band to the conduction band. At high Zn doping ($X = 0.7$ and 1.0), $In(OH)_ySz$:Zn displays an absorption edge similar to that of ZnS. Absorption bands with shoulders in the visible light region are also observed. These absorption shoulders are characteristic of doped photocatalysts [34–36] and indicate that a discontinuous level is formed by the dopants in the forbidden band.

3.3. Photoactivity of $In(OH)_ySz$ and $In(OH)_ySz$:Zn

Table 1 lists the photocatalytic H_2 production on $In(OH)_ySz$ loaded with 2wt% Pt. Both the weight loss seen on TGA and the band gap estimated from the absorption edge decrease with increasing S/In in the synthesis solution. The decreased band gap is ascribed to the more negative energy level of S 3p in contrast to O 2p. $In(OH)_3$ with a wide band gap (5.17 eV) shows no photoactivity even under UV illumination. This is because the Xe lamp that we used irradiates photons with wavelengths >300 nm, too little energy to excite the electron transition from the valence band to the conduction band of $In(OH)_3$. In contrast, $In(OH)_ySz$ can be excited by visible light because of its narrowed band gap. The photocatalytic reaction on $In(OH)_ySz$ can be described as follows [37,38]:

$$\text{photocatalyst} + h\nu \rightarrow e^-(CB) + h^+(VB) \quad \text{(photoexcitation)};$$

$$\left.\begin{aligned} 2H^+ + 2e^- &\rightarrow H_2 \\ PtCl_6^{2-} + 4e^- &\rightarrow Pt + 6Cl^- \end{aligned}\right\} \text{ Conduction band}$$

(Cocatalyst Pt deposition and water reduction);

Table 2
The physical parameter of $In(OH)_ySz$:Zn (S/In = 2.0) and the photoactivity of H_2 production under visible light illumination ($\lambda > 420$ nm)

The value of X[a]	ICP result (atomic ratio of Zn/In)	Bang gap[b] (eV)	BET surface area (m^2/g)	The rate of H_2 production[c] (μmol/h)
0	0	2.19	36.8	1.4
0.05	0.04	2.25	46.6	4.7
0.1	0.08	2.34	38.1	26.6
0.2	0.18	2.43	32.4	35.8
0.4	0.39	2.54	68.9	49.0
0.5	0.48	2.58	91.8	67.0
0.7	0.62	2.57	78.6	40.3
1.0	0.89	2.64	97.5	14.9

[a] X denoted the atomic ratio of Zn/In in the synthesis solution.
[b] Band gap estimated from the onset of the absorption edge.
[c] The average rate in 10 h photoreaction.

$$\left.\begin{aligned} SO_3^{2-} + H_2O + 2h^+ &\rightarrow SO_4^{2-} + 2H^+ \\ SO_3^{2-} + 2S^{2-} + 2h^+ &\rightarrow S_2O_3^{2-} \end{aligned}\right\} \text{ Valence band}$$

(The oxidation of the sacrificial regents).

In the initial stage, the H_2PtCl_6 in the solution is reduced to Pt^0 on surface of $In(OH)_ySz$ as the H_2 evolution promoter. After the induction period, H_2 is produced with the reduction of water molecules by the photogenerated electrons on the conduction band. Sacrificial regents SO_3^{2-} and S^{2-} are oxidized by the holes on the valence band to produce SO_4^{2-} and $S_2O_3^{2-}$ [37,38]. Although the rate of H_2 production is low (0.9–1.8 μmol/h), all $In(OH)_ySz$ catalyst with varying S/In ratios are active for H_2 production under visible light illumination. The low activity suggests that a very low thermodynamic potential for the water reduction on $In(OH)_ySz$ catalyst, consistent with the result of density functional theory calculations [22].

Table 2 lists the physical parameters and photoactivities of $In(OH)_ySz$:Zn catalysts in 0.43 M Na_2S–0.5 M Na_2SO_3 aqueous solution under visible light illumination. With X increasing from 0 to 1.0, the band gap increased from 2.19 to 2.64 eV. The Zn/In atomic ratio by inductively coupled plasma elemental analysis was close to, but slightly lower than that in the synthesis solution. The $In(OH)_ySz$:Zn with low Zn^{2+} doping had no efficient increase in BET surface area. The high doping of Zn^{2+} increased the surface area of the $In(OH)_ySz$:Zn. The photoactivity of H_2 production was more effective on $In(OH)_ySz$:Zn than on $In(OH)_ySz$. The average rate of H_2 production on $In(OH)_ySz$:Zn increased with increasing X and reached the maximum rate of 67 μmol/h when $X = 0.5$, and then declined to 40.3 and 14.9 μmol/h with $X = 0.7$ and 1.0, respectively. Fig. 6 shows the time course of H_2 production on 2wt% Pt-loaded $In(OH)_ySz$ and $In(OH)_ySz$:Zn ($x = 0.2$ and 0.5) under visible light illumination. Photocatalytic H_2 production increased steadily with increasing illumination time on both $In(OH)_ySz$ and $In(OH)_ySz$:Zn. The average rates were 35.8 and 67 μmol/h at $X = 0.2$ and 0.5, respectively. XRD analysis revealed no observable difference between the sample before and after photoreaction, suggesting that $In(OH)_ySz$:Zn is a stable photocatalyst for the reduction of water in the presence of Na_2S and Na_2SO_3.

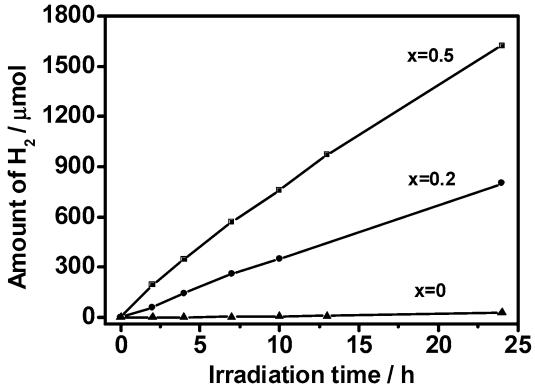

Fig. 6. Time courses of photocatalytic H_2 production from 0.43 M Na_2S–0.5 M Na_2SO_3 aqueous solution under visible light illumination on 2wt% Pt loaded $In(OH)_yS_z$ (S/In = 2) and $In(OH)_yS_z$:Zn ($x = 0.2$ and 0.5 with S/In = 2). Catalyst, 0.3 g; light source, 300 W Xe lamp with cutoff filter ($\lambda > 420$ nm).

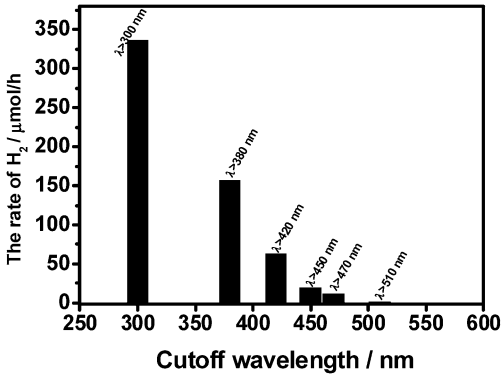

Fig. 7. Dependence of the rate of photocatalytic H_2 production on $In(OH)_yS_z$:Zn ($x = 0.5$) on the cutoff wavelength of incident light.

The dependence of the rate of H_2 on the cutoff wavelength of incident light on $In(OH)_yS_z$:Zn ($X = 0.5$) catalyst was investigated, as shown in Fig. 7. The rate of H_2 production decreased with increasing cutoff wavelength. H_2 could be photocatalytically produced even when a cutoff filter of 510 nm was used. This wavelength corresponds to the onset of the absorption edge of $In(OH)_yS_z$:Zn. However, when the illumination wavelength was >550 nm, H_2 production ceased. This finding is in accordance with the absorption edge as shown in Fig. 5.

4. Discussion

It is well known that the light absorption capability of semiconductors and the position of the conduction band are crucial factors influencing the photoactivity of H_2 production. For photocatalytic H_2 production from water, it is thermodynamically indispensable that the level of conduction band be more negative than the reduction potential of H^+/H_2. The band structure of a transition metal oxide is generally defined by the d-orbital of metal cation with a d^0 electronic configuration or the sp-orbital of metal cation with a d^{10} electronic configuration [39]. But for metal sulfide containing a metal ion with a d^{10} electronic configuration, the conduction band and valence band are determined mainly by the s- and p-orbitals of the metal cations and the S 3p orbital. The lower rate of H_2 production on $In(OH)_yS_z$ is due to the slightly higher energy level of In 5s5p over the reduction potential of H^+/H_2 [22]. The improved photoactivity of $In(OH)_yS_z$:Zn cannot be ascribed exclusively to the increased surface area. The surface area of $In(OH)_yS_z$:Zn ($X = 0.2$) is slightly less than that of $In(OH)_yS_z$, but the rate of H_2 production on $In(OH)_yS_z$:Zn ($X = 0.2$) is 35.8 μmol/h, 25 times higher than that on $In(OH)_yS_z$ (0.9–1.8 μmol/h). With $X = 0.5$, the surface area of $In(OH)_yS_z$:Zn is 91.8 m^2/g, three times larger than that of $In(OH)_yS_z$; however, the average rate of H_2 production on $In(OH)_yS_z$:Zn ($x = 0.5$) is 48 times higher than that on $In(OH)_yS_z$. Thus, it can be confirmed that the increase in surface area after Zn^{2+} doping is not the crucial factor leading to improved photoactivity.

It has been reported that the energy level of Zn 4s4p is more negative than that of In 5s5p [22]. Solid solution $(AgIn)_xZn_{2(1-x)}S_2$ photocatalysts, the conduction bands of which comprise Zn 4s4p hybridized with In 5s5p, show high activity for H_2 production in the visible region. In our work, the In 5s5p of lower energy level hybridizes with Zn 4s4p of higher energy and constitutes the new conduction band of $In(OH)_yS_z$:Zn. The conduction band of $In(OH)_yS_z$:Zn, consisting of hybridized In 5s5p with Zn 4s4p, has more negative energy level than the conduction band of $In(OH)_yS_z$, consisting of In 5s5p. This is in accordance with the blue shift of the absorption edge, as shown in Fig. 5. The elevated conduction band increases the thermodynamic driving force for water reduction. So the elevated conduction band level after Zn^{2+} doping is considered the key factor for enhancing photoactivity. It should be noted that although the thermodynamic driving force for water reduction is increased, the rate of H_2 at high Zn^{2+} doping ($X > 0.5$) is decreased. This decreased activity is partially related to the reduced number of photons available for the electron excitation because the band gap of $In(OH)_yS_z$:Zn increases at high Zn^{2+} doping. Furthermore, the doping of Zn^{2+} with high amount into the crystal lattice of $In(OH)_yS_z$ induces greater distortion of its crystal lattice. This is evident from the large shift of the diffraction peaks toward higher angles at high values of X in Fig. 2. The distorted crystal structure has a negative influence on the mobility of the charge carrier [40], leading to a decreased number of photogenerated electrons in the reduction reaction of water molecules.

According to the foregoing results, the possible band structure of $In(OH)_yS_z$:Zn is suggested and illustrated in Fig. 8. The narrowed band gap of $In(OH)_yS_z$ is attributed to the substitution of OH^- with S^{2-}. Theoretical calculations indicate that the band structure of indium oxide is dominated by O 2p and In 5s [41,42]. Thus, the conduction band and valence band of $In(OH)_yS_z$ consist predominately of In 5s5p and O 2p hybridized with S 3p, respectively. With increased X, the absorption of $In(OH)_yS_z$ shifts to the UV region, suggesting that the doped Zn^{2+} elevates the conduction band of $In(OH)_yS_z$:Zn because of the greater negative energy level of Zn 4s4p compared with In 5s5p. This change leads to a shift in the conduction band of $In(OH)_yS_z$:Zn to a more negative position and a widening of the band gap. The elevated conduction band of $In(OH)_yS_z$:Zn increases the thermodynamic driving force for water reduction at low X ($\leqslant 0.5$). The decreased number of photons and the

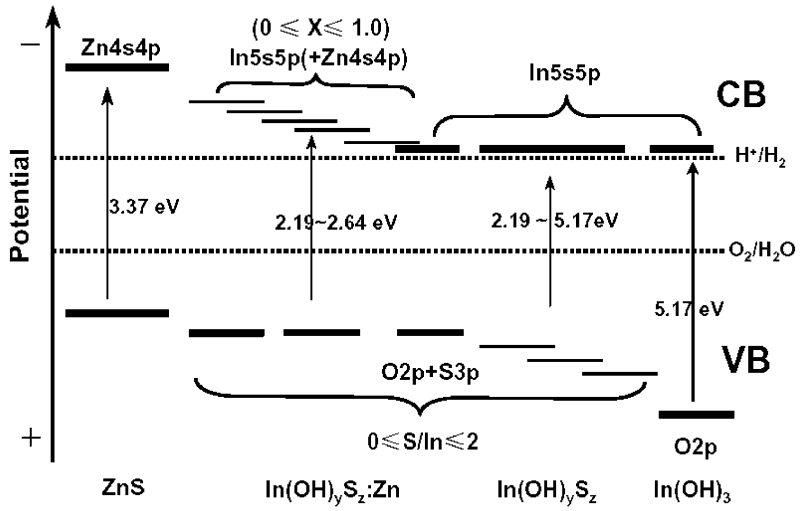

Fig. 8. The proposed band structure of $In(OH)_3$, $In(OH)_yS_z$ and $In(OH)_yS_z$:Zn.

greater distortion of crystal lattice at high X (>0.5) are responsible for the low photoactivity.

5. Conclusions

Visible light-driven $In(OH)_yS_z$ and $In(OH)_yS_z$:Zn photocatalyst were successfully synthesized via the hydrothermal method at 180 °C in an aqueous solution of ethylenediamine. The band gap of $In(OH)_3$ was narrowed by the substitution of S^{2-} for OH^-, and the absorption edge of $In(OH)_yS_z$ was dependent on the amount of S^{2-} substituted. The absorption edge of $In(OH)_yS_z$:Zn monotonously shifted to the UV region with an increasing amounts of Zn^{2+} doped. $In(OH)_yS_z$ catalyst was active for H_2 production from Na_2S–Na_2SO_3 solution under visible light illumination, and its photoactivity was further enhanced by doping with Zn^{2+}. According to the variation in absorption and photoactivity of the catalysts, a band structure of $In(OH)_yS_z$:Zn is proposed in which the valence band is composed mainly of S 3p hybridized with O 2p orbits, with the conduction band composed of In 5s5p orbits hybridized with Zn 4s4p. The more negative conduction band level consisting of In 5s5p and Zn 4s4p provides a large thermodynamic driving force for the reduction of water to produce H_2.

$In(OH)_yS_z$:Zn represents a new class of visible light-responsive metal hydroxide photocatalyst with d^{10} electronic configuration. The method outlined in this paper also provides some useful ideas for the design of other new types of metal hydroxide photocatalysts working in the visible region by combining anion substitution and cation doping.

Acknowledgments

This work was supported by the National Natural Science Foundation of China (grants 20403018, 90210036, and 20273070), the National Key Basic Research and Development Program (grant 2003CB214500), and the Solution-Oriented Research for Science and Technology (SORST) Program of Japan Science and Technology Corporation (JST). The authors thank Dr. Yunqi Qian, Institute of Chemistry for Functionalized Materials, Liaoning Normal University, for the English revision.

References

[1] H. Kato, K. Asakura, A. Kudo, J. Am. Chem. Soc. 125 (2003) 3082.
[2] N. Sato, H. Nishiyama, Y. Inoue, J. Phys. Chem. B 105 (2001) 6061.
[3] K. Ikarashi, J. Sato, H. Kobayashi, N. Saito, H. Nishiyama, Y. Inoue, J. Phys. Chem. B 106 (2003) 9048.
[4] J. Sato, N. Saito, Y. Yamada, K. Maeda, T. Takata, J.N. Kondo, M. Hara, H. Kobayashi, K. Domen, J. Am. Chem. Soc. 127 (2005) 4150.
[5] D.W. Hwang, H.G. Kim, J. Kim, K.Y. Cha, Y.G. Kim, J.S. Lee, J. Catal. 193 (2000) 40.
[6] J.W. Tang, Z.G. Zou, J.H. Ye, Angew. Chem. Int. Ed. 43 (2004) 4463.
[7] H.G. Kim, D.W. Hwang, L.S. Lee, J. Am. Chem. Soc. 126 (2004) 8912.
[8] R. Asahi, T. Morikawa, T. Ohwaki, K. Aoki, Y. Taga, Science 293 (2001) 269.
[9] S. Khan, M. Al-Shahry, W. Ingler, Science 297 (2002) 2243.
[10] S. Ito, R. Thampi, P. Comte, P. Liska, M. Grätzel, Chem. Commun. (2005) 268.
[11] M. Hara, J. Nunoshige, T. Takata, J.N. Kondo, K. Domen, Chem. Commun. (2003) 3000.
[12] W.J. Chun, A. Ishikawa, H. Fujisawa, T. Takata, J.N. Kondo, M. Hara, M. Kawai, Y. Matsumoto, K. Domen, J. Phys. Chem. B 107 (2003) 1798.
[13] M.Y. Liu, W.S. You, Z.B. Lei, G.H. Zhou, J.J. Yang, G.P. Wu, G.J. Ma, G.Y. Luan, T. Takata, M. Hara, K. Domen, C. Li, Chem. Commun. (2004) 2192.
[14] A. Ishikawa, T. Takata, J.N. Kondo, M. Hara, H. Kobayashi, K. Domen, J. Am. Chem. Soc. 124 (2002) 13547.
[15] A. Kudo, M. Sekizawa, Catal. Lett. 58 (1999) 241.
[16] A. Kudo, M. Sekizawa, Chem. Commun. (2000) 1371.
[17] I. Tsuji, A. Kudo, J. Photochem. Photobiol. A Chem. 156 (2003) 249.
[18] Z.G. Zou, J.H. Ye, K. Sayama, H. Arakawa, Nature 414 (2001) 625.
[19] Z.B. Lei, W.S. You, M.Y. Liu, G.H. Zhou, T. Takata, M. Hara, K. Domen, C. Li, Chem. Commun. (2003) 2142.
[20] A. Kudo, I. Tsuji, H. Kato, Chem. Commun. (2002) 1958.
[21] A. Ishikawa, Y. Yamada, T. Takata, J.N. Kondo, M. Hara, K. Domen, Chem. Mater. 15 (2003) 4442.
[22] I. Tsuji, H. Kato, H. Kobayashi, A. Kudo, J. Am. Chem. Soc. 126 (2004) 13406.
[23] I. Tsuji, H. Kato, A. Kudo, Angew. Chem. Int. Ed. 44 (2005) 3565.
[24] M. Wakamura, K. Hashimoto, T. Watanabe, Langmuir 19 (2003) 3428.
[25] R. Bayón, C. Guillen, M.A. Martinez, M.T. Gutierrez, J. Herrero, J. Electrochem. Soc. 145 (1998) 2775.

[26] R. Bayón, J. Herrero, Thin Solid Films 387 (2001) 111.
[27] R. Bayón, C. Maffiotte, J. Herrero, Thin Solid Films 353 (1999) 100.
[28] D. Hariskos, M. Ruckh, U. Ruhle, T. Walter, H.W. Schock, J. Hedstrom, L. Stolt, Sol Energy Mater. Sol. Cells 41–42 (1996) 345.
[29] D. Braunger, D. Hariskos, T. Walter, H.W. Schock, Sol Energy Mater. Sol. Cells 40 (1996) 97.
[30] H.L. Zhou, Y. Wang, N.Y. Wang, Y. Li, J. Yang, Mater. Lett. 58 (2004) 2631.
[31] X.H. Zhang, S.Y. Xie, Z.M. Ni, X. Zhang, Z.Y. Jiang, Z.X. Xie, R.B. Huang, L.S. Zheng, Inorg. Chem. Commun. 6 (2003) 1445.
[32] Q. Tang, W.J. Zhou, W. Zhang, S.M. Qu, K. Jiang, W.C. Yu, Y.T. Qian, Cryst. Growth Des. 5 (2005) 147.
[33] S. Avivi, Y. Mastai, A. Gedanken, Chem. Mater. 12 (2000) 1229.
[34] R. Konta, T. Ishii, H. Kato, A. Kudo, J. Phys. Chem. B 108 (2004) 8992.
[35] H. Kato, A. Kudo, J. Phys. Chem. B 106 (2002) 5029.
[36] M. Miyauchi, M. Takashio, H. Tobimatsu, Langmuir 20 (2004) 232.
[37] J.F. Reber, K. Meier, J. Phys. Chem. 88 (1984) 5903.
[38] J.F. Reber, M. Rusek, J. Phys. Chem. 90 (1986) 824.
[39] D.E. Scaife, Sol. Energy 25 (1980) 41.
[40] Z.G. Zou, J.H. Ye, H. Arakawa, Chem. Mater. 13 (2001) 1765.
[41] H. Odaka, S. Iwata, N. Taga, S. Ohnishi, Y. Kaneta, Y. Shigesato, Jpn. J. Appl. Phys. 36 (9a) (1997) 5551.
[42] C. Schinzer, F. Heyd, S.F. Mater, J. Mater. Chem. 9 (1999) 1569.